Hindawi
Mathematical Problems in Engineering
Volume 2019, Article ID 6919176, 13 pages
https://doi.org/10.1155/2019/6919176

Research Article

Analysis of Gas Flow Behavior for Highly Deviated Wells in Naturally Fractured-Vuggy Carbonate Gas Reservoirs

Kongjie Wang,[1] Lian Wang,[1] Caspar Daniel Adenutsi,[2] Zhiping Li ,[1] Sen Yang,[1] Liang Zhang,[1] and Lan Wang[1]

[1] *School of Energy Resources, China University of Geosciences, Beijing, China*
[2] *Institute of Industrial Research, Council for Scientific and Industrial Research, P.O. Box LG 576, Accra, Ghana*

Correspondence should be addressed to Zhiping Li; lzp_cugb@163.com

Received 12 May 2019; Revised 25 June 2019; Accepted 2 July 2019; Published 29 July 2019

Academic Editor: P. H. Wen

To improve the carbonate gas reservoir development and production, highly deviated wells (HDW) are widely used in the field. Production decline analysis of HDW is crucial for long-term gas reservoir development. However, it is a new challenge to incorporate the complex pore structure of naturally fractured-vuggy carbonate gas reservoirs and evaluate the production performance of HDW. This paper presents a semianalytical model to analyze the pressure and production behavior of HDW in naturally fractured-vuggy carbonate gas reservoirs, which consist of fractures, vugs, and matrix. The primary flow occurs only through the fracture and the outer boundary is closed. Introducing pseudopressure and pseudotime, the Laplace transformation, Fourier transformation, and its inverse and Stehfest numerical inversion were employed to establish a point source and line source solutions. Furthermore, the validity of the proposed model was verified by comparing a field data from the Arum River Basin in Turkmenistan. Finally, the effects of major parameters on the production decline curves were analyzed by using the proposed model and it was found that they had influences at different stages of gas production history and the sensitivity intensity of each parameter was different. With its high efficiency and simplicity, this semianalytical model will serve as a useful tool to evaluate the well production behavior for the naturally fractured-vuggy carbonate gas reservoirs.

1. Introduction

Carbonate gas reservoirs are widely distributed throughout the world. In these carbonate reservoirs, the original gas in place (OGIP) and gas production account for more than half of gas reserves and production in the world [1]. Carbonate gas reservoirs commonly have extremely complex porous structures. This mainly comprises three types of pores, which are matrix, natural fractures, and vugs with different degrees of development. Thus, gas flow in carbonate gas reservoirs show characteristics of multiple-porosity system [2]. To improve gas reservoir development and production, highly deviated wells (HDW) are widely used [3]. A new challenge that arises from the application of this technology to improve reservoir development is the difficulty in analyzing and predicting the production behaviors of HDW in naturally fractured-vuggy carbonate gas reservoirs.

In the past decades, a lot of researchers reported some relevant works. The theory and applications on dual-porosity flow model for fractured reservoirs have been well researched [4–8]. The dual-porosity model was first proposed by Warren and Root in which it was assumed that the reservoir has matrix blocks with low permeability but high porosity and the fracture system with high permeability but low porosity [9]. Based on this model, Bourdet and Gringarten introduced a log-log analysis model with wellbore storage and skin in dual-porosity systems [10]. Jalali and Ershaghi established a pressure transient model for carbonate reservoirs on semilog plots and found that the slope characteristics of the transition cover an embracing spectrum [11]. Ei-Banbi extended previous analytical models to develop a catalog of linear flow causes, models, and solutions for dual-porosity linear reservoirs, dual-porosity radial reservoirs, and dual-porosity channel reservoirs [12]. Ying-Lan et al. represented a dual-porosity

model within a porous-vuggy carbonate reservoir that does not introduce the fracture system [13].

Reservoirs composed of matrix, fracture, and vugs are called triple-porosity systems. A lot of triple-porosity models have been proposed through analytical, semianalytical, and numerical methods for analyzing gas flow in fractured-vuggy carbonate reservoirs. With regard to analytical methods, a triple-porosity and single-permeability model was first proposed by Abdassah and Ershaghi [14]. The authors considered an unsteady-state interporosity flow model between the fractures and the others, which is a more realistic representation. Al-Ghamdi and Ershaghi presented a triple-porosity dual-permeability model to characterize fracture heterogeneities, which considered discontinuous matrix and two continuous fracture networks, microfractures and macrofractures [15]. Later, another triple-porosity dual-permeability model was proposed to characterize vuggy porosity, coexisting with matrix and fractures in carbonate reservoir by Camacho-Velázquez et al. [16]. Wu et al. presented an analytical method for pressure transient analysis in fractured-vuggy carbonate reservoir that relied on a triple-continuum concept [17]. Lately, Wang et al. developed a model for transient flow analysis of acid fracturing wells in fractured-vuggy carbonate reservoirs [18]. With regard to semianalytical and numerical methods, Gulbransen et al. proposed a multiscale mixed finite element method for modeling fractured-vuggy carbonate reservoirs [19]. Li et al. built a coupled Stoked-Darcy model for estimating the equivalent permeability tensor and modeling two-phase flow with a full permeability tensor in a fracture-vug- media system [20]. Zhang et al. presented a new numerical model that considered the effect of geomechanics on fractures and vugs [21]. For upscaling fractured-vuggy reservoir models, Gao et al. introduced a numerical model that consisted of four different porosity systems, i.e., the matrix, fractures, isolated vugs, and connected vugs [22].

A substantial amount of research has focused on the pressure behavior and production performance of deviated wells. Abbaszadeh and Hegeman first proposed analytical solution for the pressure drawdown behavior of a deviated limited-entry well with different combinations of boundaries. The authors used the method of source and Green's functions to derive these solutions [23]. Ozkan and Raghavan presented a solution for a deviated limited-entry well in an infinite reservoir with no-flow top and bottom boundaries by employing the Laplace transformation [24]. Harmohan et al. introduced a method of numerical simulation to analyze the pressure transient behavior of deviated wells that intersect high permeability layers between two low permeability layers [25]. Based on rigorous derivation, Wang et al. presented a transient pressure solution for deviated wells, which reduced the amount of computation and significantly improved the computational efficiency [26]. In a recent work, Meng et al. proposed a semianalytical model of HDW for evaluating the pressure behavior which considered the stress-sensitive performance in fractured-vuggy carbonate gas reservoirs with composite systems [27]. Zhao et al. built a new model for evaluating inflow performance of HDW in anisotropic reservoirs, which was proposed by introducing the anisotropic quantitative characterization method [28].

Currently, only few suitable analytical models exist to evaluate the production behavior of HDW in fractured-vuggy carbonate gas reservoirs. In this study, a semianalytical flow model was established by employing Laplace transformation, Fourier transformation and inversion, Stehfest numerical inversion algorithm, and point source function. Based on the proposed model, the effects of major parameters on production performance were studied.

2. Physical Model

Figure 1 shows a schematic for HDW in a fractured-vuggy carbonate gas reservoir. Fractured-vuggy carbonate gas reservoirs are naturally structured by matrix system, natural fractures system, and vugs system. Figure 2 shows the physical modeling scheme of a fractured-vuggy carbonate medium. In order to mathematically define the gas flow behavior, the assumptions of this model are listed as follows:

(1) HDW are located in a laterally infinite gas reservoir.

(2) The gas reservoir is assumed to be horizontal with equal thickness and have two impermeable boundaries at the top and bottom.

(3) During the well production, gas flows only through the fracture system into the wellbore; interporosity flow occurs from the vugs and the matrix systems to the fracture system.

(4) Flow is single phase, isothermal and follows Darcy's law. Gravitational and capillary effects are negligible.

(5) The pressure is uniform initially throughout the gas reservoir and is equal to p_i.

(6) The HDW produces at a constant rate q_g or at constant pressure p_{wf}.

(7) The permeability k_h in horizontal direction and k_z in vertical direction are different.

3. Mathematical Model

3.1. Establishment of Mathematical Model. In this work, the interporosity flow from vugs and matrix to fractures is assumed to be pseudosteady state. Combining the continuity equation with transport equation as well as the equation of state and the introduction of pseudopressure and pseudotime (the detailed procedure for pseudopressure and pseudotime is documented in Appendix A), the governing equation for the triple-porosity system in radial cylindrical coordinate is given as follows:

$$\frac{1}{r}\frac{\partial}{\partial r}\left(r\frac{\partial m_f}{\partial r}\right)+\frac{k_{vf}}{k_f}\frac{\partial^2 m_f}{\partial z^2} = \frac{1}{0.0864}\frac{\phi_f \mu_g C_{tf}}{k_{hf}}\frac{\partial m_f}{\partial t_p}-\alpha_m\frac{k_m}{k_h}\left(m_m-m_f\right) - \alpha_c\frac{k_c}{k_h}\left(m_c-m_f\right) \quad (1)$$

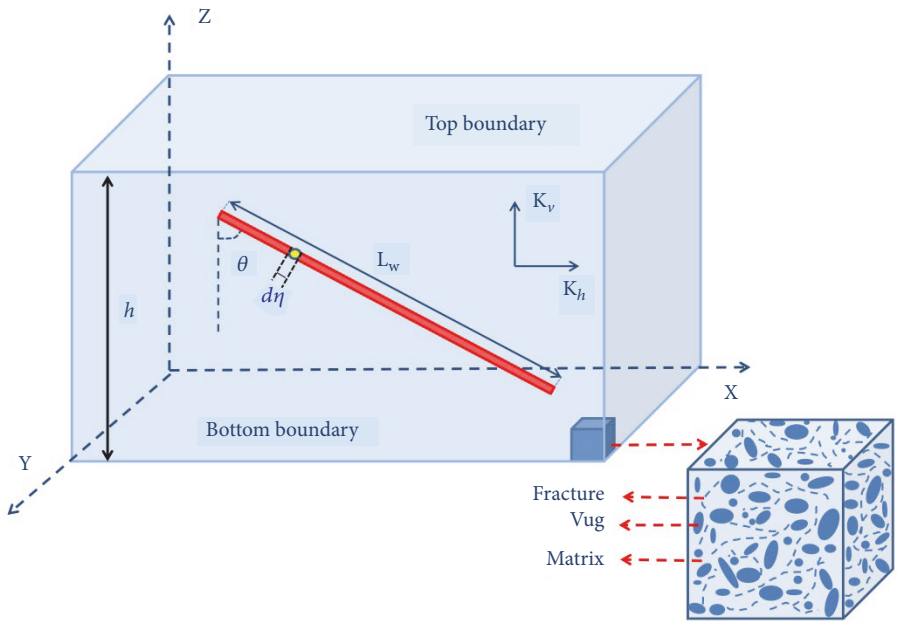

Figure 1: Schematic diagram of HDW in a fractured-vuggy carbonate gas reservoir.

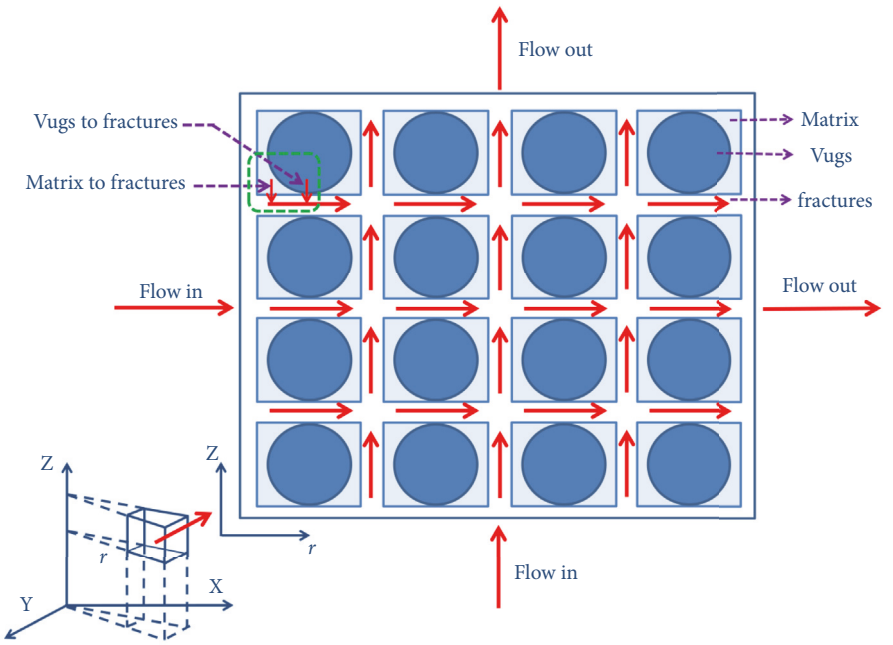

Figure 2: Flow sketch map for a cell [29].

For the matrix system the equation is

$$\frac{\phi_m \mu_g C_{tm}}{0.0864} \frac{\partial m_m}{\partial t_p} = \alpha_m k_m \left(m_f - m_m\right) \tag{2}$$

For the vugs system the equation is

$$\frac{\phi_c \mu_g C_{tc}}{0.0864} \frac{\partial m_c}{\partial t_p} = \alpha_c k_c \left(m_f - m_c\right) \tag{3}$$

where m_f, m_m, m_c is the pseudopressure of fractures system, matrix system, vugs system, respectively, MPa/s; ϕ_f, ϕ_m, ϕ_c is porosity of fracture system, matrix system, vugs system, respectively, fraction; k_f, k_m, k_c is permeability of fracture system, matrix system, vugs system, respectively, md; k_{vf} is vertical fracture permeability, md; C_{tf}, C_{tm}, C_{tc} is compressibility of fracture system, matrix system, vugs system, respectively, MPa^{-1}; μ_g is gas viscosity, $mPa \cdot s$; α_m,

α_c are shape factors of matrix and vugs, $1/m^2$; and t_p is pseudotime, day.

The initial pseudopressure m_i is assumed uniform for the triple-porosity system:

$$m_j(r, t=0) = m_i, \quad (j = f, m, c) \tag{4}$$

The outer boundary is closed:

$$\left.\frac{\partial m_j}{\partial r}\right|_{r=r_e} = 0, \quad (j = f, m, c) \tag{5}$$

At the inner boundary, there is a continuous point source (x_w, y_w, z_w) with a constant gas rate $\tilde{q}$:

$$\tilde{q}B_{gi} = \begin{cases} \lim\limits_{\varepsilon\to 0}\left(\lim\limits_{r\to 0}\dfrac{k_{hf}}{\alpha_p\mu_g\varepsilon}\displaystyle\int_{z_w-\varepsilon/2}^{z_w+\varepsilon/2} r\frac{\partial m_f}{\partial r}dz\right) & |z-z_w| \le \dfrac{\varepsilon}{2} \\ 0 & |z-z_w| > \dfrac{\varepsilon}{2} \end{cases} \tag{6}$$

where k_{hf} is fracture horizontal permeability, md.

At the top and bottom, the boundaries are impermeable:

$$\left.\frac{\partial m_f}{\partial z}\right|_{z=0} = \left.\frac{\partial m_f}{\partial z}\right|_{z=h} = 0 \tag{7}$$

where h is formation thickness, m.

Based on the definitions of dimensionless variables in Table 1, the governing equations and the initial and boundary conditions (Eq. (1)-(7)) can be transformed into dimensionless terms (Eq. (8)-(14)).

The dimensionless governing equation of fracture, matrix, and vugs systems are

$$\frac{1}{r_D}\frac{\partial}{\partial r_D}\left(r_D\frac{\partial m_{fD}}{\partial r_D}\right) + \frac{\partial^2 m_{fD}}{\partial {z_D}^2} = \omega_f\frac{\partial m_{fD}}{\partial t_D} - \lambda_m\left(m_{mD} - m_{fD}\right) - \lambda_c\left(m_{cD} - m_{fD}\right) \tag{8}$$

$$\omega_m\frac{\partial m_{mD}}{\partial t_D} = \lambda_m\left(m_{fD} - m_{mD}\right) \tag{9}$$

$$\omega_c\frac{\partial m_{cD}}{\partial t_D} = \lambda_c\left(m_{fD} - m_{cD}\right) \tag{10}$$

Transformed initial condition:

$$m_{jD}(r_D, t_D = 0) = 0, \quad (j = f, m, c) \tag{11}$$

Transformed outer boundary condition:

$$\left.\frac{\partial m_{jD}}{\partial r_D}\right|_{r_D=r_{eD}} = 0, \quad (j = f, m, c) \tag{12}$$

Transformed inner boundary condition:

$$\lim_{\varepsilon_D\to 0}\left(\lim_{r_D\to 0}\int_{z_{wD}-\varepsilon_D/2}^{z_{wD}+\varepsilon_D/2} r_D\frac{\partial m_{fD}}{\partial r_D}dz_D\right) = \begin{cases} -h_D & |z_D - z_{wD}| \le \dfrac{\varepsilon_D}{2} \\ 0 & |z_D - z_{wD}| > \dfrac{\varepsilon_D}{2} \end{cases} \tag{13}$$

Transformed top and bottom boundaries:

$$\left.\frac{\partial m_{fD}}{\partial z_D}\right|_{z_D=0} = \left.\frac{\partial m_{fD}}{\partial z_D}\right|_{z_D=h_D} = 0 \tag{14}$$

3.2. Solution of Mathematical Model

3.2.1. Basic Continuous Point Source Solution. Laplace transformation, Fourier transformation, and inversion were employed to solve the dimensionless model (Eq. (8)-(14)). The solution in Laplace space is as follows (the detailed procedure for the solution is documented in Appendix B).

$$\begin{aligned} \overline{m}_{fD} = {} & \frac{1}{s}\left[\frac{K_1\left(r_{eD}\sqrt{sf(s)}\right)}{I_1\left(r_{eD}\sqrt{sf(s)}\right)}I_0\left(r_D\sqrt{sf(s)}\right) + K_0\left(r_D\sqrt{sf(s)}\right)\right] + \frac{2}{s} \\ & \cdot\sum_{n=1}^{\infty}\left[\frac{K_1\left(r_{eD}\sqrt{u_n^2 + sf(s)}\right)}{I_1\left(r_{eD}\sqrt{u_n^2 + sf(s)}\right)}I_0\left(r_D\sqrt{u_n^2 + sf(s)}\right) + K_0\left(r_D\sqrt{u_n^2 + sf(s)}\right)\right]\cos\left(\mu_n z_{wD}\right)\cos\left(\mu_n z_D\right) \end{aligned} \tag{15}$$

where

$$u_n = \frac{n\pi}{h_D} \tag{16}$$

$$f(s) = w_f + \frac{\lambda_c\omega_c}{\lambda_c + \omega_c s} + \frac{\lambda_m\omega_m}{\lambda_m + \omega_m s} \tag{17}$$

where k_0 is modified Bessel function of zero order of the second kind; k_1 is modified Bessel function of order one of the second kind; I_0 is modified Bessel function of order zero of the first kind; I_1 is modified Bessel function of order one of the first kind.

3.2.2. Pressure Distribution of a HDW. To obtain the pressure solution of HDWs, the wellbore was treated as a uniform flux line source. It was assumed that there was an infinitesimal point on the HDW. Based on the principle of superposition for a point source, integration was carried out along the deviated line for the line source solution. Cinco (1975) successfully got the r, θ, z-coordinates of the equivalent-pressure point where the wellbore pressure of HDW can be calculated easily [30]. Therefore, the dimensionless pressure distribution of HDW in Laplace domain is given as follows:

$$\begin{aligned}\overline{m}_{fD} &= \frac{1}{sL_{wD}}\int_{-L_{wD}/2}^{L_{wD}/2}\left[\frac{K_1\left(r_{eD}\sqrt{sf(s)}\right)}{I_1\left(r_{eD}\sqrt{sf(s)}\right)}I_0\left(\widetilde{r}_D\sqrt{sf(s)}\right)+K_0\left(\widetilde{r}_D\sqrt{sf(s)}\right)\right]d\eta \\ &+\frac{2}{sL_{wD}}\int_{-L_{wD}/2}^{L_{wD}/2}\left\{\sum_{n=1}^{\infty}\left[\frac{K_1\left(r_{eD}\sqrt{u_n^2+sf(s)}\right)}{I_1\left(r_{eD}\sqrt{u_n^2+sf(s)}\right)}I_0\left(\widetilde{r}_D\sqrt{u_n^2+sf(s)}\right)+K_0\left(\widetilde{r}_D\sqrt{u_n^2+sf(s)}\right)\right]\right. \\ &\left.\cdot\cos\left(\mu_n\widetilde{z}_{wD}\right)\cos\left(\mu_n z_D\right)\right\}d\eta\end{aligned} \tag{18}$$

where

$$\widetilde{r}_D = \sqrt{\left(x_D - x_{wD} - \eta\sin\theta_w\right)^2 + \left(y_D - y_{wD}\right)^2} \tag{19}$$

$$\widetilde{z}_{wD} = z_{wD} + \eta\cos\theta_w \tag{20}$$

$$\theta_w = \tan^{-1}\left(\sqrt{\frac{k_{vf}}{k_{hf}}}\tan\theta\right) \tag{21}$$

$$L_{wD} = \frac{L_w}{r_w}\sqrt{\frac{k_f}{k_{hf}}\sin^2\theta + \frac{k_f}{k_{vf}}\cos^2\theta} \tag{22}$$

Based on the principle of superposition, the pressure solution with wellbore storage and skin effect in Laplace domain can be obtained as

$$\overline{m}_{wD} = \frac{s\overline{m}_{fD} + S}{s + C_D s^2\left(s\overline{m}_{fD} + S\right)} \tag{23}$$

$$C_D = \frac{C}{6.28\left(\phi C_t\right)_{f+c+m}hr_w^2} \tag{24}$$

where C is wellbore storage coefficient, m^3/MPa; $\overline{m}_{wD}$ is the dimensionless bottom pseudopressure.

3.2.3. Gas Production Based on the Well Pressure Responses. According to Van Everdingen and Hurst [31], the dimensionless production response for a HDW producing at a constant bottom-hole pressure in the Laplace domain can be obtained as follows:

$$\overline{q}_{wD} = \frac{1}{s^2\overline{m}_{wD}} \tag{25}$$

Equation (25) can then be inverted to obtain q_{wD} in real space using suitable numerical inversion algorithms such as Stehfest's inversion algorithm [32].

4. Results and Discussion

4.1. Proposed Model Application and Validation. Field data from the Arum River Basin in Turkmenistan was used to validate the proposed model and to demonstrate its practical application. Arum River Basin is a large scale sedimentary basin, which is located between the border of Turkmenistan and Uzbekistan. The reservoir bed possesses carbonate rock that is formed by postdepositional diagenesis, including dissolution and dolomitization. Vugs, fractures, and dissolution pores are highly dispersed in the reservoir. The details of relevant parameters needed for the model evaluation are listed in Table 2. These parameters are obtained by various methods in the field. In particular, it should be noted that formation radius (r_e), fracture permeability (k_f), interporosity flow coefficients between different media systems (λ_c, λ_m), and initial reservoir pressure (p_i) can be obtained through interpretation of well testing data. And the porosity of three different media (ϕ_f, ϕ_m, ϕ_c) can be obtained by combining well logging data with core CT scanning.

Figure 3 shows a comparison between daily rate of gas production from a highly deviated well from the field and simulated gas production rate from the proposed model. It was found that the proposed model had a good fitting with actual production data. Except for very few data points that deviated from the simulated curve due to the real production time being less than 24 hours, the rest of the data fits well with the curve. After ignoring data points less than 24 hours of production, the average relative error (E) between the remaining actual data and model data is only 4.19%. The average relative error (E) is evaluated by

$$E = \frac{1}{n}\sum_{j=1}^{n}\frac{\left|q_{gj} - \widetilde{q_{gj}}\right|}{\widetilde{q_{gj}}} \tag{26}$$

where q_{gi} is simulated production rate from the proposed model, m^3/d; $\widetilde{q_{gj}}$ is field production rate, m^3/d.

Moreover, it could be seen that the trend of simulated production rate in the following 1000 days and even longer predicted the gas production trend for the future with a constant bottom-hole pressure. Based on this application, it

Table 1: Definitions of dimensionless variables.

Dimensionless variables	Definitions
Dimensionless pseudopressure	$m_{jD} = \dfrac{\pi k_f h T_{sc}\left[m_i(p_i) - m_j(p)\right]}{p_{sc} q_g T} \quad (j = f, m, c)$
Dimensionless pseudotime	$t_D = \dfrac{\alpha_t k_f t_p}{\mu_g r_w^2 (\phi C_t)_{f+m+c}}$
Dimensionless radius	$r_D = \dfrac{r}{r_w}\sqrt{\dfrac{k_f}{k_{hf}}}$
Dimensionless formation radius	$r_{eD} = \dfrac{r_e}{r_w}\sqrt{\dfrac{k_f}{k_{hf}}}$
Dimensionless distance of x coordinate	$x_D = \dfrac{x}{r_w}\sqrt{\dfrac{k_f}{k_{hf}}}$
Dimensionless distance of y coordinate	$y_D = \dfrac{y}{r_w}\sqrt{\dfrac{k_f}{k_{hf}}}$
Dimensionless distance of mid-perforation in x coordinate	$x_{wD} = \dfrac{x_w}{r_w}\sqrt{\dfrac{k_f}{k_{hf}}}$
Dimensionless distance of mid-perforation in y coordinate	$y_{wD} = \dfrac{y_w}{r_w}\sqrt{\dfrac{k_f}{k_{hf}}}$
Dimensionless formation thickness	$h_D = \dfrac{h}{r_w}\sqrt{\dfrac{k_f}{k_{hf}}}$
Dimensionless vertical distance	$z_D = \dfrac{z}{r_w}\sqrt{\dfrac{k_f}{k_{hf}}}$
Dimensionless vertical distance of mid-perforation	$z_{wD} = \dfrac{z_w}{r_w}\sqrt{\dfrac{k_f}{k_{hf}}}$
Dimensionless infinitesimal variable	$\varepsilon_D = \dfrac{\varepsilon}{r_w}\sqrt{\dfrac{k_f}{k_{hf}}}$
Dimensionless deviated well length	$L_{wD} = \dfrac{L_w}{r_w}\sqrt{\dfrac{k_f}{k_{hf}}\sin^2\theta + \dfrac{k_f}{k_{vf}}\cos^2\theta}$
Dimensionless storativity ratio	$\omega_j = \dfrac{\phi_j C_{tj}}{(\phi C_t)_{f+m+c}}, \quad (j = f, m, c)$
Dimensionless interporosity flow coefficient	$\lambda_j = \dfrac{\alpha_j k_j r_w^2}{k_f}, \quad (j = m, c)$
Dimensionless production rate	$q_{wD} = \dfrac{p_{sc} T}{\pi T_{sc} k_f h\left[m_i(p_i) - m_w(p_{wf})\right]} q_g$

is confirmed that the proposed model can be used to describe the gas production behavior of HDW in naturally fractured-vuggy carbonate gas reservoir. Therefore, the estimated input parameters of the model will be used as the basis for the sensitivity analysis.

4.2. Modeling of Production Behavior with Triple-Porosity Flows. In order to understand the production behavior with triple-porosity flows, different flow regime analysis was conducted to study the effects of various flow mechanisms on the overall production behavior. Figure 4 shows the complete transient flow process of HDW production in fractured-vuggy carbonate gas reservoir under closed circle boundary and it can be divided into five flow stages. The first stage was dominated by wellbore storage and skin effect and the dimensionless pseudopressure and pseudopressure derivative curves showed a straight line with a slope of 1. After that, skin factor affected the shape of the derivative curve that looked like a "hump". The second stage was dominated by inclination angle (θ) of HDW. When the inclination angle approached 0°, the HDW was treated as a vertical well. In this case, this stage would not be obvious or would completely disappear on the curve. The third stage was dominated by interporosity flow between fractures and vugs and this flow regime behaved with a "dip" on the pressure derivative curve. Because the gas flow in the vugs was relatively smoother

Table 2: The values of relevant parameters for verification and sensitivity analysis.

Parameters	Value
Wellbore radius, r_w (m)	0.0889
Formation radius, r_e (m)	400
Formation thickness, h (m)	30
Fracture permeability, k_f (m)	1
Interporosity flow coefficient between fractures and vugs, λ_c	2×10^{-4}
Interporosity flow coefficient between fractures and matrix, λ_m	2×10^{-6}
Fractures porosity, ϕ_f	0.002
Matrix porosity, ϕ_m	0.04
Vugs porosity, ϕ_c	0.017
Inclination angle, θ (°)	75
Length of the highly deviated well, L_w (m)	300
Initial reservoir pressure, p_i (MPa)	24
Bottom-hole pressure, p_w (MPa)	20
Reservoir temperature, T (K)	381.15
Gas production rate, q_g (m^3/d)	600,000
Gas viscosity, μ_g (mPa·s)	0.02
Gas compressibility factor, Z (m^3/m^3)	0.97

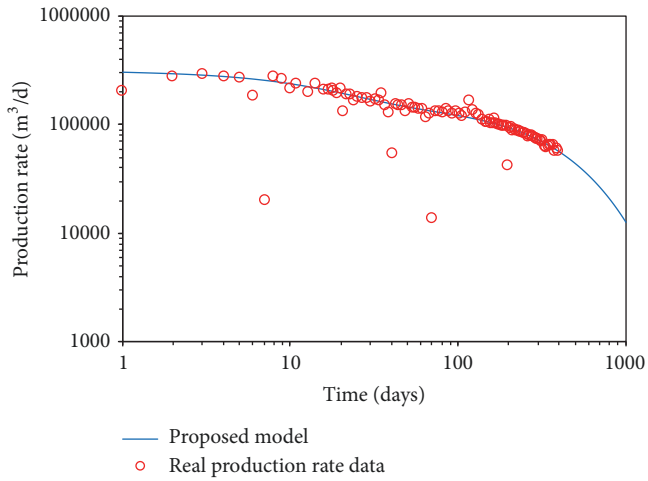

Figure 3: Comparing simulated results and production rates of Arum River Basin HDW.

than in the matrix, the interporosity flow between fractures and vugs appeared first when the wellbore pressure began to deplete. Therefore, wellbore pressure depletion was retarded due to gas supplement from vugs to fracture system. The fourth stage was dominated by interporosity flow between fractures and matrix and this stage also behaved with a "dip" on the pressure derivative curve. It is worth noting that the third and fourth stages could interfere with each other, depending on the value of λ_c and λ_m. The fifth stage was dominated by closed circle boundary, which manifested on the derivative curve with a slope of 1.

4.3. Model Sensitivity Analyses. Based on the field data, the production sensitivity analyses for different key parameters are discussed. In this section, the HDW produces with a constant bottom-hole pressure. The key parameters include formation thickness, fracture permeability, inclination angle of the HDW, formation radius, interporosity flow coefficient between fractures and vugs and vugs storativity ratio. The influences of these parameters are apparent and their estimates are essential for future production analysis and forecasting.

Figure 5 shows the effects of formation thickness on production performance. From Figure 5, it can be seen that formation thickness primarily influences every stage of gas production. For the time, $t < 100$ days, the difference of gas production rates between different formation thicknesses were almost the same. It meant that the decline rates of gas production for different scenarios were almost the same. After the time, $t > 100$ days, the differences become smaller with increase in time. In addition, it was also observed that with decrease in formation thickness, the area enclosed

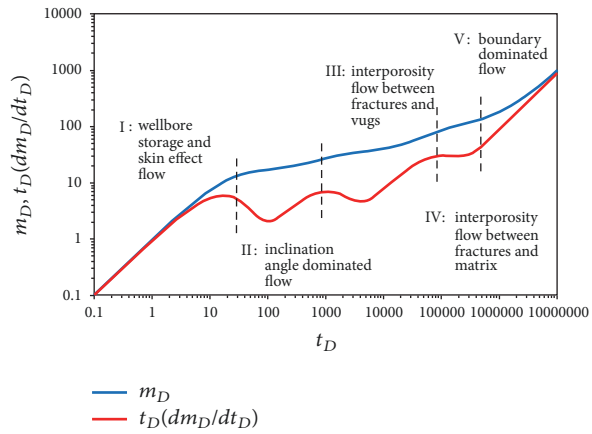

Figure 4: Typical pressure curves for HDW in fractured-vuggy carbonate gas reservoir under closed circle boundary.

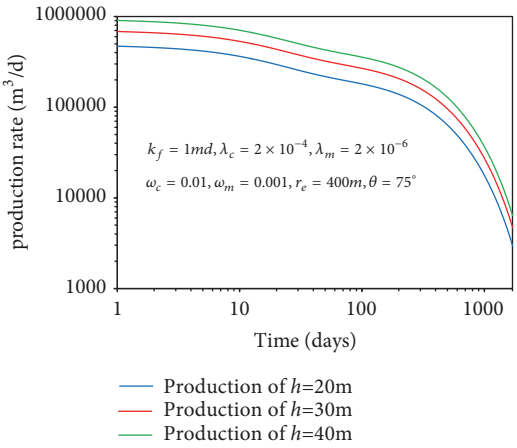

Figure 5: Effect of formation thickness on production decline curves.

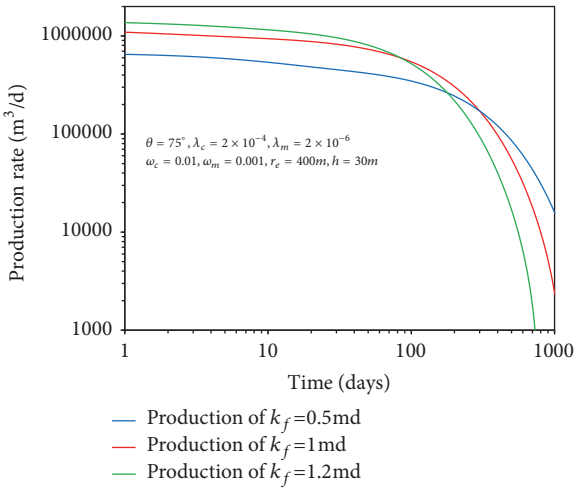

Figure 6: Effect of fracture permeability on production decline curves.

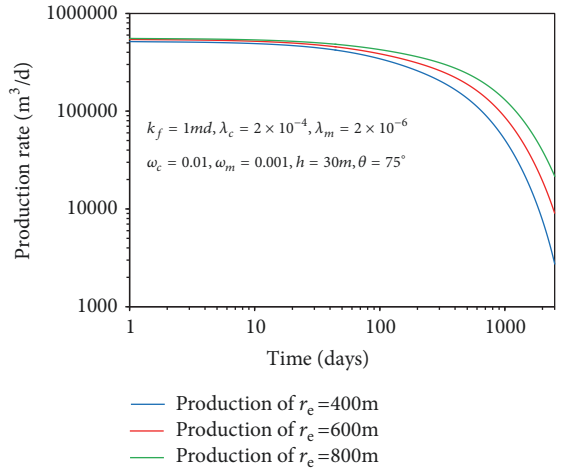

Figure 7: Effect of gas reservoir radius on production decline curves.

by the curve became smaller, which meant the cumulative production reduced.

From Figure 6, it was noted that permeability affects the whole period of gas production. The higher the fracture permeability, the higher the initial production rate. However, for a reservoir with higher fracture permeability, production rate would decrease drastically, and during the middle-late stages the production rate would be exceeded by a reservoir with lower fracture permeability. Moreover, a well with low fracture permeability has a long stable production period.

Figure 7 shows the effects of reservoir radius on gas production performance of HDWs. The difference of gas production at late stage was increasingly wider. It was noted that with increase in gas reservoir radius, the production curves declined more gently, which meant a gas reservoir with bigger radius would have a longer stable production period.

Figure 8 shows the effects of interporosity flow coefficient between fractures and vugs on gas production performance of the HDW. It can be seen that the coefficient primarily affected early stage of gas production. For the time, $t < 10$ days, with the interporosity flow coefficient between fractures

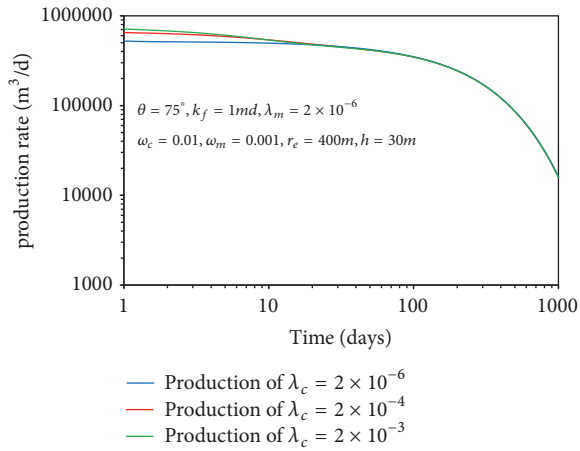

FIGURE 8: Effect of interporosity flow coefficient between fractures and vugs on production decline curves.

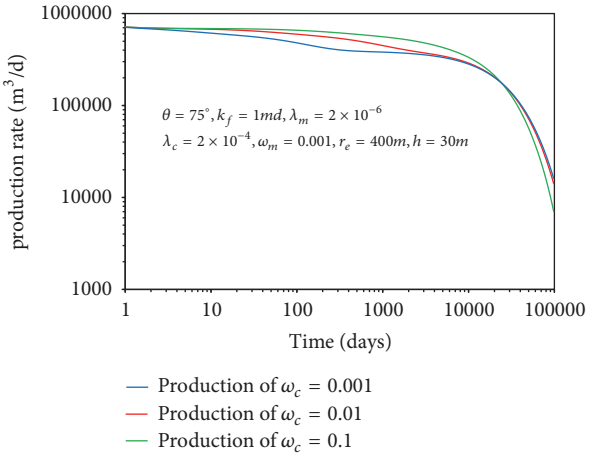

FIGURE 9: Effect of vugs storativity ratio on production decline curves.

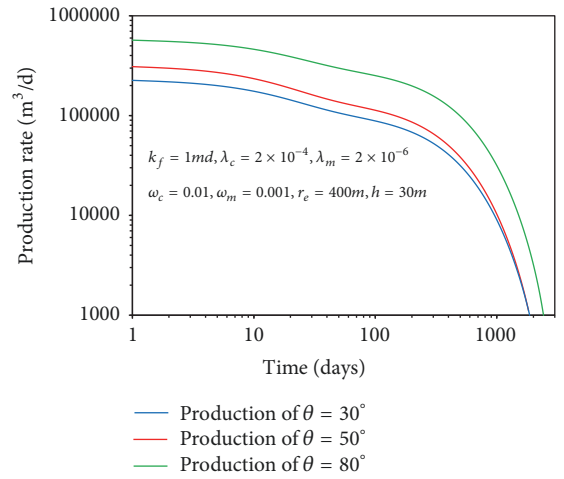

FIGURE 10: Effect of inclination angle on production decline curves.

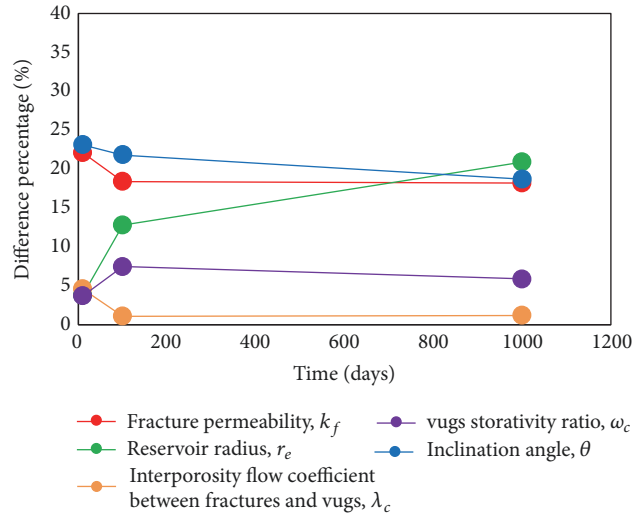

FIGURE 11: Trends of percentage difference of parameters by extracting production rate at t=10 days, 100 days, 1000 days.

and vugs smaller, the initial production also became smaller and the production rate decreased relatively slower. For the time, $t > 10$ days, there was no difference between the production rates of the three scenarios. From Figure 9, it was observed that vugs storativity ratio affected middle-late stage of gas production. During $10 < t < 10000$ days, with vugs storativity ratio smaller, production rate decreased more rapidly. However, after $t > 10000$ days, the difference in the production curves was contrary to the previous one. Meanwhile, it was obvious that the extent of production variation is less drastic than the middle stage.

Figure 10 shows the effects of the angle of inclination on gas production performance of the HDW. It can be seen that the angle of inclination also affects the entire stage of gas production. Due to the effects of different inclination angle on contact area of wellbore, the cumulative gas production increases with increase in inclination angle.

According to Figures 5–10, the production decline curve was affected by many parameters and the intensity of production variation was different at different stages of gas production history. By extracting production rate data at different times (t=10days, 100days, 1000days) for adjacent parameters in Table 3, production difference percentage (Δq_{per}) could be obtained which could be helpful in comparing the sensitivity of these parameters.

Based on Table 3, trends of difference in percentage of parameters are shown in Figure 11. It can be seen that the bigger the difference in percentage value, the more sensitive the parameters. Inclination angle (θ) and fracture permeability (k_f) seemed to be the two most sensitive parameters; reservoir radius (r_e) was the third, vugs storativity ratio (ω_c) and interporosity flow coefficient between fractures and vugs (λ_c) were the least two sensitive parameters.

Table 3: Effect of parameters at t=10 days, 100 days, 1000 days on the difference in production rate percentage.

parameters		10 days Δq_{per}, %	100 days Δq_{per}, %	1000 days Δq_{per}, %
k_f, md	1/0.5	22.1	18.4	18.2
r_e, m	800/400	3.8	12.8	20.9
λ_c	0.0002/0.00002	4.6	1.1	1.2
ω_c	0.1/0.01	3.7	7.5	5.9
θ, degree	80/40	23.1	21.8	18.7

5. Conclusions

This research investigated the production decline behavior of highly deviated well (HDW) in naturally fractured-vuggy carbonate gas reservoir. The validity of the proposed model was verified by matching it with the production history of a field case from the Arum River carbonate gas reservoir in Turkmenistan. Furthermore, the effects of relevant parameters on production performance were studied. The main conclusions drawn are as follows:

(1) The proposed production semianalytical model could be used to predict the gas production trend with a constant bottom-hole pressure.

(2) Pressure type curves for HDW in naturally fractured-vuggy carbonate gas reservoir were divided into five flow stages. Among them, the second stage was dominated by the inclination angle (θ) of the HDW. The third stage was dominated by interporosity flow between fractures and vugs. The fourth stage was dominated by interporosity flow between fractures and matrix. However, the third and fourth stages could interfere with each other, depending on the values of λ_c and λ_m.

(3) Using the proposed model, sensitivity analyses were conducted and it was found that formation thickness (h), fracture permeability (k_f), inclination angle of the HDW affected the entire stage of gas production history. Interporosity flow coefficient between fractures and vugs (λ_c) affected the early stage of gas production history. Vugs storativity ratio affected middle-late stage of gas production history. Gas reservoir radius affected late stage of gas production history. Moreover, inclination angle (θ) seemed to be the most sensitive parameter, fracture permeability (k_f) was the second most sensitive parameter, followed by reservoir radius (r_e), while vugs storativity ratio (ω_c) and interporosity flow coefficient between fractures and vugs (λ_c) were the last two sensitive parameters.

Appendix

A. Calculation of Pseudopressure and Pseudotime

In (1)- (7), m_f, m_m, m_c is the pseudopressure of the fracture system, matrix system, and vugs system, respectively, MPa/s; t_p is pseudotime, day. The pseudopressure and pseudotime can be given as follows:

$$m = \int_0^p \frac{2p}{\mu_g Z} dp \tag{A.1}$$

$$t_p = \int_0^t \frac{1}{\mu_g C_t} dt \tag{A.2}$$

B. Calculation of Continuous Point Source Solution

Equations (8)-(14) can be transformed into Laplace domain by the Laplace transformation.

The dimensionless governing equations of fractures, matrix, and vugs systems in the Laplace domain are as follows:

$$\begin{aligned} &\frac{1}{r_D}\frac{\partial}{\partial r_D}\left(r_D \frac{\partial \overline{m}_{fD}}{\partial r_D}\right) + \frac{\partial^2 \overline{m}_{fD}}{\partial {z_D}^2} \\ &\quad = \omega_f s\overline{m}_{fD} - \lambda_m\left(\overline{m}_{mD} - \overline{m}_{fD}\right) \\ &\qquad - \lambda_c\left(\overline{m}_{cD} - \overline{m}_{fD}\right) \end{aligned} \tag{B.1}$$

$$\omega_m s\overline{m}_{mD} = \lambda_m\left(\overline{m}_{fD} - \overline{m}_{mD}\right) \tag{B.2}$$

$$\omega_c s\overline{m}_{cD} = \lambda_c\left(\overline{m}_{fD} - \overline{m}_{cD}\right) \tag{B.3}$$

The outer boundary condition is transformed as

$$\left.\frac{\partial \overline{m}_{jD}}{\partial r_D}\right|_{r_D = r_{eD}} = 0, \quad (j = f, m, c) \tag{B.4}$$

The inner boundary condition is transformed as

$$\begin{aligned} &\lim_{\varepsilon_D \longrightarrow 0}\left(\lim_{r_D \longrightarrow 0}\int_{z_{wD}-\varepsilon_D/2}^{z_{wD}+\varepsilon_D/2} r_D \frac{\partial \overline{m}_{fD}}{\partial r_D} dz_D\right) \\ &\quad = \begin{cases} -\dfrac{h_D}{s} & \left|z_D - z_{wD}\right| \le \dfrac{\varepsilon_D}{2} \\ 0 & \left|z_D - z_{wD}\right| > \dfrac{\varepsilon_D}{2} \end{cases} \end{aligned} \tag{B.5}$$

The top and bottom boundaries are transformed as

$$\left.\frac{\partial \overline{m}_{fD}}{\partial z_D}\right|_{z_D=0} = \left.\frac{\partial \overline{m}_{fD}}{\partial z_D}\right|_{z_D=h_D} = 0 \tag{B.6}$$

where

$$\overline{m}_{jD} = \int_0^{\infty} e^{-st_D} m_{jD}(t_D)\, dt_D, \quad (j = f, m, c) \tag{B.7}$$

To eliminate the variable z_D in the governing equation, (B.1)-(B.5) can be transformed by Fourier cosine transform. The Fourier cosine transform and inverse Fourier cosine transform are given as follows:

$$\widehat{m}_{jD} = \int_0^{h_D} m_{jD} \cos\left(\frac{n\pi z_D}{h_D}\right) dh_D, \quad (j = f, m, c) \tag{B.8}$$

$$m_{jD} = \sum_n \widehat{m}_{jD} \frac{\cos\left(n\pi z_D/h_D\right)}{N(n)}, \quad (j = f, m, c) \tag{B.9}$$

where

$$N(n) = \int_0^{h_D} \cos^2\left(\frac{n\pi z_D}{h_D}\right) dz_D = \begin{cases} h_D & n = 0 \\ \dfrac{h_D}{2} & n = 1, 2, 3 \ldots \end{cases} \tag{B.10}$$

By employing the Fourier cosine transform (Eq. (B.8)), Eqs. (B.1)-(B.5) can be transformed as follows:

$$\frac{d^2\widehat{\overline{m}}_{fD}}{dr_D^2} + \frac{1}{r_D}\frac{d\widehat{\overline{m}}_{fD}}{dr_D} - \left[u_n^2 + sf(s)\right]\widehat{\overline{m}}_{fD} = 0 \tag{B.11}$$

where

$$u_n = \frac{n\pi}{h_D} \tag{B.12}$$

$$f(s) = w_f + \frac{\lambda_c \omega_c}{\lambda_c + \omega_c s} + \frac{\lambda_m \omega_m}{\lambda_m + \omega_m s} \tag{B.13}$$

The outer boundary condition is transformed as

$$\left.\frac{\partial \widehat{\overline{m}}_{jD}}{\partial r_D}\right|_{r_D = r_{eD}} = 0, \quad (j = f, m, c) \tag{B.14}$$

The inner boundary condition is transformed as

$$\lim_{r_D \to 0} r_D \frac{\partial \widehat{\overline{m}}_{fD}}{\partial r_D} = -\frac{h_D}{s}\cos\left(u_n z_{wD}\right) \tag{B.15}$$

Then (B.11) can be transformed to a modified Bessel function of zero order, like the following:

$$\left(r_D\sqrt{u_n^2 + sf(s)}\right)^2 \frac{d^2\widehat{\overline{m}}_{fD}}{d\left(r_D\sqrt{u_n^2 + sf(s)}\right)^2} + r_D\sqrt{u_n^2 + sf(s)}\frac{d\widehat{\overline{m}}_{fD}}{d\left(r_D\sqrt{u_n^2 + sf(s)}\right)} - r_D^2\left(u_n^2 + sf(s)\right)\widehat{\overline{m}}_{fD} = 0 \tag{B.16}$$

The general solution of (B.16) is given as follows:

$$\widehat{\overline{m}}_{fD} = A_0 I_0\left[r_D\sqrt{u_n^2 + sf(s)}\right] + B_0 K_0\left[r_D\sqrt{u_n^2 + sf(s)}\right] \tag{B.17}$$

Based on the outer and inner boundary conditions (Eq. (B.14)-(B.15)), the solution in Laplace domain can be obtained by inverse Fourier cosine transform as follows:

$$\overline{m}_{fD} = \frac{1}{s}\left[\frac{K_1\left(r_{eD}\sqrt{sf(s)}\right)}{I_1\left(r_{eD}\sqrt{sf(s)}\right)} I_0\left(r_D\sqrt{sf(s)}\right) + K_0\left(r_D\sqrt{sf(s)}\right)\right] + \frac{2}{s} \cdot \sum_{n=1}^{\infty}\left[\frac{K_1\left(r_{eD}\sqrt{u_n^2 + sf(s)}\right)}{I_1\left(r_{eD}\sqrt{u_n^2 + sf(s)}\right)} I_0\left(r_D\sqrt{u_n^2 + sf(s)}\right) + K_0\left(r_D\sqrt{u_n^2 + sf(s)}\right)\right]\cos\left(\mu_n z_{wD}\right)\cos\left(\mu_n z_D\right) \tag{B.18}$$

Nomenclature

C:	Wellbore storage coefficient, m^3/MPa
C_t:	Total compressibility, MPa^{-1}
E:	Average relative error, %
h:	Formation thickness, m
k:	Permeability of vugs system, md
L_w:	High deviated well length, m
m:	Pseudopressure, MPa
m_w:	Well bottom-hole pseudopressure, MPa
p:	Pressure, MPa
p_{wf} :	Well bottom-hole pressure, MPa
p_{sc}:	Pressure at standard condition, MPa
$\widetilde{q}$:	Production rate from point source, m^3/d
q_g:	Gas production rate, m^3/d
q_{gj}:	Simulated production rate from the proposed model, m^3/d
$\widetilde{q_{gj}}$:	Field production rate, m^3/d
r:	Radial distance, m
r_w:	Wellbore radius, m
r_e:	Formation radius, m
S:	Skin factor
s:	Laplace transform variable
t:	Pseudotime, day
t_p:	Pseudotime, day
T:	Reservoir temperature, k
T_{sc}:	Temperature at standard condition, k
x, y, z:	Directional coordinates

x_w, y_w, z_w: Distance of mid-perforation in x, y, and z coordinates, m
Z: Z-factor of gas, dimensionless
α_c, α_m: Shape factors of vugs and matrix, $1/m^2$
λ: Interporosity flow coefficient, dimensionless
ω: Storativity ratio, dimensionless
θ: Inclination angle, degree
ϕ: Porosity, fraction
μ_g: Gas viscosity, $mPa{\cdot}s$
α_p: Constant, $\alpha_p = 1.842$

Subscript

c: Vugs system
f: Fractures system
m: Vugs system
h: Horizontal direction
i: Initial condition
j: Initial condition
v: Vertical direction
D: Dimensionless.

Superscript

$\bar{}$: Laplace domain
$\hat{}$: Fourier domain
$\tilde{}$: Field production data.

Data Availability

The field data from the Arum River Basin in Turkmenistan used to support the findings of this study are included within the article.

Conflicts of Interest

The authors declare that they have no conflicts of interest.

Acknowledgments

The authors would like to acknowledge the support provided by Xin Zhao and Jun Shi in the initial stages of this study. This article is funded by National Science and Technology Major Project of China (*Grant Nos.* 2017ZX05030-003 *and* 2017ZX05009-005).

References

[1] L. Yong, W. Qi, L. Baozhu, and L. Zhiliang, "Dynamic characterization of different reservoir types for a fractured-caved carbonate reservoir," in *Proceedings of the SPE Kingdom of Saudi Arabia Annual Technical Symposium and Exhibition, SPE-188113-MS*, pp. 390–403, Dammam, Saudi Arabia, April 2017.

[2] P. Yue, Z. Xie, S. Huang, H. Liu, S. Liang, and X. Chen, "The application of N2 huff and puff for IOR in fracture-vuggy carbonate reservoir," *Fuel*, vol. 234, pp. 1507–1517, 2018.

[3] P. Ghahri and M. Jamiolahmady, "A new, accurate and simple model for calculation of productivity of deviated and highly deviated well – Part I: Single-phase incompressible and compressible fluid," *Fuel*, vol. 97, pp. 24–37, 2012.

[4] H. Kazemi, "Pressure transient analysis of naturally fractured reservoirs with uniform fracture distribution," *SPE Journal*, vol. 9, no. 4, pp. 451–462, 1969.

[5] K. Serra, A. Reynolds, and R. Raghavan, "New pressure transient analysis methods for naturally fractured reservoirs," *Journal of Petroleum Technology*, vol. 35, no. 12, pp. 2271–2283, 1983.

[6] R. D. Evans, "A proposed model for multiphase flow through naturally fractured reservoirs," *SPE Journal*, vol. 22, no. 05, pp. 669–680, 1982.

[7] A. O. Igbokoyi and D. Tiab, "Well test analysis in naturally fractured reservoirs using elliptical flow," in *Proceedings of the International Petroleum Technology Conference 2007, IPTC 2007*, pp. 150–165, Dubai, UAE, December 2007.

[8] B. Gao, Z. Huang, J. Yao, X. Lv, and Y. Wu, "Pressure transient analysis of a well penetrating a filled cavity in naturally fractured carbonate reservoirs," *Journal of Petroleum Science and Engineering*, vol. 145, pp. 392–403, 2016.

[9] J. E. Warren and P. J. Root, "The behavior of naturally fractured reservoirs," *SPE Journal*, vol. 3, no. 3, pp. 245–255, 1963.

[10] D. Bourdet and A. C. Gringarten, "Determination of fissure volume and block size in fractured reservoirs by type-curve analysis," in *Proceedings of the SPE annual technical conference and exhibition, SPE-9293-MS*, Dallas, Tex, USA, September 1980.

[11] Y. Jalali and I. Ershaghi, "Pressure transient analysis of heterogeneous naturally fractured reservoirs," in *Proceedings of the SPE California Regional Meeting, SPE-16341-MS*, pp. 175–188, Ventura, Calif, USA, April 1987.

[12] A. H. El-Banbi, *Analysis of tight gas well performance [Ph.D. thesis]*, Texas A&M University, Texas, Tex, USA, 1999.

[13] Y. Jia, X. Fan, R. Nie, Q. Huang, and Y. Jia, "Flow modeling of well test analysis for porous–vuggy carbonate reservoirs," *Transport in Porous Media*, vol. 97, no. 2, pp. 253–279, 2013.

[14] D. Abadassah and I. Ershaghi, "Triple-porosity systems for representing naturally fractured reservoirs," *SPE Formation Evaluation*, vol. 1, no. 2, pp. 113–127, 1986.

[15] A. Al-Ghamdi and I. Ershaghi, "Pressure transient analysis of dually fractured reservoirs," *SPE Journal*, vol. 1, no. 1, pp. 93–100, 1996.

[16] R. Camacho-Velazquez, M. Vasquez-Cruz, R. Castrejon-Aivar, and V. Arana-Ortiz, "Pressure transient and decline curve behaviors in naturally fractured vuggy carbonate reservoirs," in *Proceedings of the SPE Annual Technical Conference and Exhibition, SPE-77689-MS*, San Antonio, Tex, USA, 2002.

[17] Y. Wu, H. Liu, and G. Bodvarsson, "A triple-continuum approach for modeling flow and transport processes in fractured rock," *Journal of Contaminant Hydrology*, vol. 73, no. 1-4, pp. 145–179, 2004.

[18] M. Wang, Z. Fan, X. Dong, H. Song, W. Zhao, and G. Xu, "Analysis of flow behavior for acid fracturing wells in fractured-vuggy carbonate reservoirs," *Mathematical Problems in Engineering*, vol. 2018, Article ID 6431910, 20 pages, 2018.

[19] A. F. Gulbransen, V. L. Hauge, and K.-A. Lie, "A multiscale mixed finite-element method for vuggy and naturally fractured reservoirs," *SPE Journal*, vol. 15, no. 2, pp. 395–403, 2010.

[20] Y. Li, J. Yao, Y. Li et al., "An equivalent continuum approach for modeling two-phase flow in fractured-vuggy media," *International Journal for Multiscale Computational Engineering*, vol. 15, no. 1, pp. 79–98, 2017.

[21] F. Zhang, M. An, B. Yan, and Y. Wang, "Modeling the depletion of fractured vuggy carbonate reservoir by coupling geomechanics with reservoir flow," in *Proceedings of the SPE Reservoir Characterisation and Simulation Conference and Exhibition, SPE-186050-MS*, Abu Dhabi, UAE, 2017.

[22] S. Gao, J. E. Killough, J. He, M. M. Fadlelmula, F. Y. Wang, and M. L. Fraim, "A new approach for the simulation of fractured vuggy carbonate reservoir with an application to upscaling," in *Proceedings of the SPE Reservoir Characterisation and Simulation Conference and Exhibition, SPE-186018-MS*, Abu Dhabi, UAE, 2017.

[23] M. Abbaszadeh and P. S. Hegeman, "Pressure-transient analysis for a slanted well in a reservoir with vertical pressure support," *SPE Formation Evaluation*, vol. 5, no. 3, pp. 277–284, 1990.

[24] E. Ozkan and R. Raghavan, "A computationally efficient, transient-pressure solution for inclined wells," in *Proceedings of the SPE Annual Technical Conference and Exhibition*, New Orleans, La, USA, 1998.

[25] H. Gill, R. Al-Zayer, and M. B. Issaka, "Pressure transient behavior of horizontal and slant wells intersecting a high-permeability layer," in *Proceedings of the SPE 15th Middle East Oil and Gas Show and Conference, MEOS 2007*, pp. 1332–1344, Manama, Bahrain, March 2007.

[26] H. Wang, L. Zhang, J. Guo, Q. Liu, and X. He, "An efficient algorithm to compute transient pressure responses of slanted wells with arbitrary inclination in reservoirs," *Petroleum Science*, vol. 9, no. 2, pp. 212–222, 2012.

[27] F. Meng, Q. Lei, D. He et al., "Production performance analysis for deviated wells in composite carbonate gas reservoirs," *Journal of Natural Gas Science and Engineering*, vol. 56, pp. 333–343, 2018.

[28] X. Zhao, H. Wang, and S. Xue, "Effective model to evaluate the inflow performance of highly deviated wells in anisotropic reservoirs," *Journal of Engineering Science and Technology Review*, vol. 11, no. 5, pp. 119–127, 2018.

[29] L. Wang, X. Chen, and Z. Xia, "A novel semi-analytical model for multi-branched fractures in naturally fractured-vuggy reservoirs," *Scientific Reports*, vol. 8, no. 1, 2018.

[30] H. Cinco-Ley, H. Ramey, and F. G. Miller, "Pseudo-skin Factors for Partially-Penetrating Directionally-Drilled Wells," in *Proceedings of the fall meeting of the society of petroleum engineers of AIME*, Dallas, Tex, USA, 1975.

[31] A. F. van Everdingen and W. Hurst, "The application of the Laplace transformation to flow problems in reservoirs," *Journal of Petroleum Technology*, vol. 1, no. 12, pp. 305–324, 1949.

[32] H. Stehfest, "Algorithm 368: Numerical inversion of Laplace transforms [D5]," *Communications of the ACM*, vol. 13, no. 1, pp. 47–49, 1970.